Virtual Wedging in Three Dimensional Peg Insertion Tasks

Robert H. Sturges, Jr., Schitt Laowattana

EDRC 24-95-92

VIRTUAL WEDGING IN THREE DIMENSIONAL PEG INSERTION TASKS

Robert H. Sturges, Jr.
Associate Professor

Department of Mechanical Engineering
Carnegie Mellon University
Pittsburgh, PA 15213

Schitt Laowattana
Research Assistant

Center of Operation for Field Robotics Development
King Mongkut's Inst. Tech. Thonburi
Bangkok, Thailand 10140

ABSTRACT

Quasi-static wedging of three-point contacts is investigated, wherein the concepts of virtual and redundant wedging due to a resultant force falling into a friction cone are proposed. We consider the fully-started case of a square peg and hole consisting of two point-surface contacts and one line-line contact. An analysis of the wedging diagram for this highly constrained configuration is carried out and compared to the two dimensional case. An approximate wedging diagram is constructed which shows that wedging of square pegs into square holes is more likely than cylindrical pegs and holes of similar sizes.

INTRODUCTION

Assembly consumes, on average, 50% of a product's in-plant cycle time and direct labor. We believe that Flexible Assembly Systems (FAS) will be highly cost effective where many styles and models of a particular product are required, due to the ease of reprogramming the machines. The various styles and models can be expected to undergo several design changes during the life cycle of the equipment. However, a truly flexible assembly environment is, at present, difficult to achieve. A more thorough understanding of Part Mating Analysis is required to be able to program with high repeatability. An example of part mating is the well known "peg-in-hole" problem, which is one of the most ubiquitous assembly operations. Using a pure positional control, the success of peg insertion requires that the part clearance is not smaller than the accuracy and/or the repeatability of the manipulators and manufacturing jigs. In addition, wear of manufacturing machines and imperfect alignment of parts are unavoidable in the manufacturing plant. Dimensions of the same component also differ from one part to another due to practical constraints such as cost and technical shortcomings. The geometrical variations, unfortunately, may cause excessive mating forces, which will then lead to the failure of the insertion process.

Assembly robots in the laboratory which use force control often operate with inherent instability. When the flexibility of the system induces a vibration within the desired closed-loop bandwidth, instability will often occur. The implementation of high-bandwidth, high-accuracy force control has proven to be difficult. This is especially due to the "contact instability" problem (Eppinger and Seering, 1987), which occurs when contact is made with a rigid environment, such as in the peg insertion process.

Whitney, et. al. (1982) established a strategy for inserting a chamfered, round peg into a round hole. This strategy assumes that the peg and hole are rigid and that the peg is mounted with a compliant structure. A special configuration of this compliant structure, Remote Center of Compliance (RCC), gives especially good characteristics in supporting the peg. It reduces the mating forces and the likelihood of jamming and wedging. In this analysis, jamming refers to failure of assembly due to improperly aligned forces; wedging refers to improper geometrical initial conditions. Caine (1985) analyzed the insertion of chamferless right rectangular pegs. In this case, there are sets of forces and moments which must be applied to the peg to avoid jamming. Strip (1988a) extended Caine's approach to include a hybrid force-position strategy using active compliance for convex three-dimensional pegs. This strategy initially tilted the peg and subsequently moved it in contact with the hole. The point of support and the target point were defined such that it would simulate human behavior. The target point was selected based on the shape of both the peg and the hole as well as the point of support on the peg. Strip (1988a) also indicated that the reduction of the degrees of freedom leads to an easier interpretation of the forces measured. Strip (1988b) also invented a passive mechanism for jamming avoidance in three-dimensional insertion. Wedging conditions were not considered.

Three-dimensional wedging was studied by Sturges (1988), but limited to two opposing contact points. This study also extended the jamming diagram of Whitney, et. al. (1982) to the three-dimensional case.

It is essential that both wedging and jamming conditions must be observed for successful peg-in-hole assembly. Wedging most likely occurs in assembly processes where initial errors cannot be measured nor guaranteed by the tolerances of mating parts. In this paper, we will investigate conditions for wedging in three dimensions and develop a corresponding wedging diagram.

WEDGING DUE TO THREE-POINT CONTACTS

There are conditions in which wedging may occur among multiple point contacts, although there is no wedging at any *pair* of contacts between the peg and hole. In the case of multi-point contacts, we classify wedging into three types: two point, virtual and redundant. The two-point wedge is described in Whitney, et. al. (1982). Virtual wedging of three-point contacts occurs when lines connecting the contact points of each pair *do not* fall within the friction cones of both contacts. However, a combination of two friction cones may form a resultant force which lies within the third friction cone. Such a wedging condition imposes geometric constraints on the forces and the contact points. Redundant wedging is created by multiple instances of two-point wedges and/or virtual wedges.

General conditions for planar wedging are shown in Fig. 1 for a polynomial shaped boundary of a planar hole. Let X_i (i = 1,2,3) be the three contact points on the surface of the hole. Their coordinates $[x_i, y_i]$ are polynomial in C_i with lateral errors, $\varepsilon_i = [c_i, c_i^{\dagger}]$. The notation of Faverjon and Ponce (1991) is particularly useful in developing the constraints for planar wedging. A contact configuration for virtual wedging is a set of C_i for which the following inequalities are satisfied:

$$(X_4 - X_3) \Theta \hat{X}_3 \quad \leq \quad \alpha \qquad (1)$$

where $X_4 = [x_4, y_4]$, the intersection of two friction cones can be determined from:

$$(X_4 - X_2) \Theta \hat{X}_2 \quad \leq \quad \alpha \qquad (2)$$

$$(X_4 - X_1) \Theta \hat{X}_1 \quad \leq \quad \alpha \qquad (3)$$

where $\hat{X}_i$: unnormalized normal to contact point i; α : half angle of friction cone; and Θ denotes the angle which associates to two corresponding vectors.

In the case of redundant wedging, a pair of virtual wedges is formed with more than one set of contacts. There are three possible pairs [i,j] of contacts: [1,2] [1,3] [2,3] . Six inequalities bound the wedging region of each pair of contacts as follows:

$$(X_i - X_j) \Theta \hat{X}_j \quad \leq \quad \alpha\,, \qquad (4)$$

$$(X_j - X_i) \Theta \hat{X}_j \quad \leq \quad \alpha\,. \qquad (5)$$

$$i = 1,2\,;\; j = i + 1$$

Figure 2 shows how to determine the value θ_{2w} which determines wedging for polygonal contact configurations. Let θ_1 and θ_3 be specified. The contact point 3 is at the origin. The following parameters are given according to the geometry of the hole.

d_2 and d_3	:	x-y coordinate of contact point 1
d_1 and d_4	:	x-y coordinate of contact point 2

The condition for a virtual wedge exists when point 4 lies within friction cone of point 3. That is, the resultant of the two forces lying on the edge of the first and second friction cones passes through point 3 and therefore lies within the third friction cone.

$$\theta_{2w} \quad = \quad \left(\frac{\pi}{2} - \alpha\right) - \tan^{-1}\left(\frac{d_1 - |I_x|}{d_4 - I_y}\right), \qquad (6)$$

where I_x and I_y are trigonometric functions of d_2 , d_3 , θ_1 and α, shown in Appendix I.

From Fig. 2, the shaded area of the friction cone at point 3 shows a possible region where reaction forces from three contacts (1, 2 and 3) are in equilibrium. One boundary of each of the three friction cones intersects at point 4 for $\theta_2 = \theta_{2w}$. Point 4 is a special condition which helps define the upper and lower limits of the wedging space. In general, point 4 does not exist, but point 4' and point 4" show the actual limits of virtual and redundant wedging. The boundaries of the first and third friction cones also intersect at point 4', whereas those of the first and second friction cones intersect at point 4". A line 4'-2 connects point 4' and 2. Angle γ is defined as an angle which the line 4'-2 makes with the line 2-4. This angle is the lower limit of θ_2 where the virtual wedging condition is satisfied as θ_2 is rotated counter clockwise. Note that every point along the line 4-4' lies within the third friction cone. We also define β as an angle between the line 4'-2 and the line 2-1. If the angle θ_2 is decreased by rotating the cone 2 in the counter clockwise direction, a reaction force from the contact point 1 will fall into the friction cone of point 2 and two-point wedging occurs. If virtual wedging and two-point wedging occur simultaneously, we have redundant wedging. Therefore, in order to have only virtual wedging, γ must be smaller than β.

The value of θ_{2w} is plotted in Fig. 3 as a function of d_4 for selected values of θ_1, θ_2 and d_1, d_2, d_3. The upper bound condition of virtual wedging is determined by adding 2α to θ_{2w}. Its lower bound condition is obtained by subtracting β from θ_{2w}. The upper bound and lower bound conditions of redundant wedging are $(\theta_{2w} - \beta)$ and $(\theta_{2w} - \beta - 2\alpha)$, respectively. To avoid wedging, θ_2 must lie outside the areas of virtual and redundant wedging.

It should be clear from Fig. 2 that a sufficient condition for virtual wedging exists if any two friction cones corresponding to two contact points both include the third contact point.

In this section, we introduced the concepts of virtual and redundant wedging in the plane. The extension to three dimensions will be described in the following sections.

FEATURE DEFINITIONS OF A SQUARE PEG AND A HOLE

Figure 4 shows a square peg and hole. All designations for bounding edges have been attached. A reference frame for the peg is designed with prime (′). The four side edges are described by line segments β_i' (i = 1, ..,4). The four bottom edges are denoted by line segments γ_i' (i = 1, ..,4). O′ is the origin of reference coordinates for the peg which is attached to the first bottom corner, p_1. Let w be the width of the peg. The point-coordinates of the four corners are

$$p_1' \quad = \quad [\,0 \quad 0 \quad 0 \quad 1\,]^t \qquad (7)$$

$$p_2' \quad = \quad [\,0 \quad w \quad 0 \quad 1\,]^t \qquad (8)$$

$$p_3' \quad = \quad [\,-w \quad w \quad 0 \quad 1\,]^t \qquad (9)$$

$$p_4' \quad = \quad [\,-w \quad 0 \quad 0 \quad 1\,]^t \qquad (10)$$

For the square hole, the four top inner edges are described by line segment α_i (i = 1, ..,4). The outer edges of the chamfer are denoted by line segment ε_i (i = 1, ..,4) and the four chamfer corners by line segment δ_i (i = 1, ..,4). It is assumed that the

inner edges lie normal to line α. O is the origin of reference coordinates for the hole which is attached to the first inside corner, q_1. If W is the width of the hole, the point coordinates of the four-hole corners will be

$$q_1 = [\,0 \quad 0 \quad 0 \quad 1\,]^t \tag{11}$$

$$q_2 = [\,0 \quad W \quad 0 \quad 1\,]^t \tag{12}$$

$$q_3 = [\,-W \quad W \quad 0 \quad 1\,]^t \tag{13}$$

$$q_4 = [\,-W \quad 0 \quad 0 \quad 1\,]^t \tag{14}$$

In addition, each chamfer surface is defined a point e_i in the plane which contain lines α_i and ϵ_i.

$$e_1 = [\,c\eta \quad 0 \quad s\eta \quad 1\,]^t \tag{15}$$

$$e_2 = [\,0 \quad c\eta+W \quad s\eta \quad 1\,]^t \tag{16}$$

$$e_3 = [\,-c\eta-W \quad 0 \quad s\eta \quad 1\,]^t \tag{17}$$

$$e_5 = [\,-w \quad -c\eta \quad s\eta \quad 1\,]^t \tag{18}$$

where η is the chamfer angle with the horizontal plane. The symbols c and s represent trigonometric functions for cosine and sine, respectively.

AN APPROXIMATE MODEL OF WEDGING FOR THE ORTHO-CONFIGURATION

Using the notation for the peg and hole defined in the previous section, we will analyze the onset of wedging with three contacts. Of the many likely contact configurations which are possible after chamfer crossing, the ortho configuration (Sturges, 1988) of Fig. 5 is typical of three-point constraints. This contact configuration consists of two point-surface contacts and a line-line contact. It is always possible to obtain this configuration during chamfer contact since there is no possibility of planar wedging for the two point contacts. However, as the peg advances to cross the chamfer, the resultant of two contacts might fall into the friction cone of the third contact (point-surface). Equations (15)-(18) are shown in the previous section for the purpose of completeness of geometrical description. The chamfer angle (η) is involved in the determination of a lateral error(ε_0) defined in Whitney, et. al. (1982). Since, at the onset of wedging for this configuration, the peg has already passed the chamfer surface, we will consider the contacts made by the geometry of the peg and hole as shown in eqs. (7)-(14). The three contacts are pictorially shown in Fig. 5 which excludes the chamfer surface. We will develop an approximate wedging diagram for this case taking the x-z plane of the hole as a reference plane and comparing it with the two-dimensional case of Whitney et. al. (1982).

For polygonal pegs and holes, contact configurations such as line-line can be analytically described by using the Plücker coordinates $[\tilde{N},\tilde{N}_0]$. $\tilde{N}$ is a directional vector which is not necessarily normalized. $\tilde{N}_0$ is a moment of a line l. P is any point on the line l.

$$\tilde{N}_0 = P \times \tilde{N}. \tag{19}$$

The contact states analysis to follow is most conveniently expressed in Plücker coordinates. Let the direction cosines of peg line β' define a unit vector $\tilde{N}'$ at infinity in frame O':

$$\tilde{N}' = [\beta_1' \quad \beta_2' \quad \beta_3' \quad 0], \tag{20}$$

which can be transformed to be a unit vector in frame O of the hole by

$$\tilde{N} = D\tilde{N}', \tag{21}$$

where D is the homogeneous transformation matrix which relates the location of the peg with respect to the hole:

$$D = \begin{bmatrix} c\psi c\phi & s\theta c\psi s\phi - s\psi c\theta & s\theta s\psi + c\theta c\psi s\phi & x_o \\ s\psi c\phi & s\theta s\psi s\phi + c\psi c\theta & c\theta s\psi s\phi - s\theta c\psi & y_o \\ -s\phi & c\phi s\theta & c\phi c\theta & z_o \\ 0 & 0 & 0 & 1 \end{bmatrix}, \tag{22}$$

In the analysis below, we will refer to the elements of D as:

$$D = \begin{bmatrix} d_{11} & d_{12} & d_{13} & x_o \\ d_{21} & d_{22} & d_{23} & y_o \\ d_{31} & d_{32} & d_{33} & z_o \\ 0 & 0 & 0 & 1 \end{bmatrix} \tag{23}$$

Contact constraints are readily described by computing the mutual moment between two lines (Hunt, 1978). The mutual moment of two lines is defined as the distance between the lines along their unique common normal multiplied by the sine of the angle between them

$$d \sin\theta = \tilde{N}_1\tilde{N}_{02} + \tilde{N}_2\tilde{N}_{01} \tag{24}$$

If the Plücker coordinates of l_1 and l_2 are:

$$l_1 = \alpha_1 \quad \alpha_2 \quad \alpha_3 \;,\; \alpha_4 \quad \alpha_5 \quad \alpha_6 \tag{25}$$

$$l_2 = \beta_1 \quad \beta_2 \quad \beta_3 \;,\; \beta_4 \quad \beta_5 \quad \beta_6 \tag{26}$$

then

$$\tilde{N}_1\tilde{N}_{02} = \alpha_1\beta_4 + \alpha_2\beta_5 + \alpha_3\beta_6 \tag{27}$$

$$\tilde{N}_2\tilde{N}_{01} = \beta_1\alpha_4 + \beta_2\alpha_5 + \beta_3\alpha_6 \tag{28}$$

From eq. (26), if p is any point on the line l, the moment part of the Plücker coordinates can be expressed in a matrix form as

$$\tilde{N}_{02} = \Lambda p = \Lambda D p' \tag{29}$$

where Λ is an antisymmetric cross-product matrix:

$$\tilde{N}_{02}N = \begin{bmatrix} 0 & \beta_3 & -\beta_2 & 0 \\ -\beta_3 & 0 & \beta_1 & 0 \\ \beta_2 & -\beta_1 & 0 & 0 \\ 0 & 0 & 0 & 1 \end{bmatrix} \tag{30}$$

At this point, we can use the Plücker coordinates to restate the line segments of the peg and hole, β_2 and α_2, which create the line-line contact at point 2 of the ortho configuration.

$$\beta_2' = (0 \quad 0 \quad 1 \quad w \quad 0 \quad 0) \tag{30}$$

$$\alpha_2 = (0 \quad 0 \quad 1 \quad 0 \quad 0 \quad -W) \tag{31}$$

These two lines satisfy the line-line contact constraint at point 2 when $z_3 = 0$. By using eqs. (24) and (29), we obtain the coordinate of point 2:

$$p_2 = D = \left[\frac{-\beta_5}{\beta_3} \quad \frac{\beta_4}{\beta_3} \quad 0 \quad 1\right]^t. \tag{32}$$

From eqs. (21), (22), and (29)-(31), the coordinate of β_2 in the reference frame of the hole is obtained:

$$\beta_2 = \begin{bmatrix} d_{13} \\ d_{23} \\ d_{33} \\ y_o d_{33} - z_o d_{23} + w d_{11} \\ z_o d_{13} - x_o d_{33} + w d_{21} \\ x_o d_{23} - y_o d_{13} + w d_{31} \end{bmatrix}. \tag{33}$$

Setting $d = 0$ in eq. (24) and substituting with eqs. (31) and (33), yields the contact constraint relation:

$$z_0(s\theta c\psi - c\theta s\psi s\phi) + (y_0 - W)c\phi c\theta + w c\phi c\psi = 0. \tag{34}$$

Figure 5 also shows the geometry for the onset of wedging (if there is one) as the second point-surface contact (point 1) enters the hole. According to Fig. 5, one can see that two point-surface contacts are located at

$$p_1 = (0 \quad y_0 \quad 0 \quad 1)^t \tag{35}$$

$$p_3 = (x_3 \quad 0 \quad z_3 \quad 1)^t \tag{36}$$

We obtain the unknown coordinate of point 1 and point 3 from eqs. (9), (22) and (36):

$$y_0 = w\,(c\psi c\theta + s\theta s\psi s\phi - s\psi c\theta) \tag{37}$$

$$x_3 = w\,(s\theta c\psi s\phi - c\psi c\phi - s\psi c\theta) \tag{38}$$

$$z_3 = w\,(c\phi s\theta - s\phi) \tag{39}$$

Since virtual wedging can exist if any of two friction cones of two contacts in Fig. 5 both include the third contact point, a set of six relationships between contact points can be found. Table 1 gives the minimum values for friction coefficient, μ, which cause wedging, based on the geometry of Fig. 5 and the analysis in Section 3 above. To read the table, consider a row number as a friction cone base and a column number as an included contact point. A virtual wedge formed by the friction cones at contact 1 and contact 3 including contact 2 (denoted as *VW(1,2)* and *VW(3,2)*) satisfies relations in row 1 - column 2 and row 3 - column 2, viz:

$$\frac{|z_3|}{\sqrt{\left[W^2 + (x_2 - x_3)^2\right]}} \leq \mu \tag{40}$$

$$\left|\frac{W - y_o}{x_2}\right| \leq \mu \tag{41}$$

Table 1 Minimum values of μ sufficient for wedging

		Included Contact Point		
		1	2	3
Friction Cone Base	1	—	$\left\|\frac{W - y_o}{x_2}\right\|$	$\left\|\frac{\sqrt{y_0^2 + z_3^2}}{x_3}\right\|$
	2	$\left\|\frac{x_2}{W - y_o}\right\|$	—	$\frac{\|z_3\|}{\sqrt{\left[W^2 + (x_2 - x_3)^2\right]}}$
	3	$\frac{\|x_3\|}{\sqrt{y_0^2 + z_3^2}}$	$\frac{\|z_3\|}{\sqrt{\left[W^2 + (x_2 - x_3)^2\right]}}$	—

Due to a small angle approximation, we assume that the normal to all three contacts is perpendicular to the inner surface of the hole. The inner surface of the hole at point 3 is parallel to one at point 2 but perpendicular to one at point 1. Therefore, *VW(2,3)* and *VW(3,2)* are the same whereas *VW(1,3)* and *VW(2,3)* are reciprocal to *VW(3,1)* and *VW(3,2)*, respectively. Replacing inequalities by equalities in eqs. (40) and eq. (41) and solving eq. (37) through eq. (41) yield the possible configurations for the onset of wedging, which we now develop into a wedging diagram.

Referring to the wedging diagram for two dimensions (Whitney et.al, 1982) in Fig. 6, the linear equation of the upper and lower boundary is

$$\theta_0 + s\varepsilon_0 < \theta_w \tag{42}$$

where θ_w, a wedging limit angle, is equal to $\pm c/\mu$.

The parameter s and c represent a slope and clearance ratio between the peg and hole, respectively:

$$s = \frac{L_g}{\left(L_g^2 + \frac{K_\theta}{K_x}\right)} \tag{43}$$

$$c = \frac{(W - w)}{W} \tag{44}$$

with

- θ_0 : angular error
- ε_0 : lateral error
- L_g : distance from a rigid support to the peg's tip
- K_x : lateral compliance
- K_θ : angular compliance

A quasi-static analysis, similar to Whitney, et. al. (1982), has been carried out relative to the x-axis of the hole for the ortho configuration of the peg. The slope and wedging limit θ_w of eq. (42) is formed using relations given by eqs. (37) through (41) and static balances of forces and moments about a compliance center defined in Whitney, et. al. (1982). After doing a bit of algebra and dropping high order terms, we find that:

$$s = \frac{L_g\left[c\theta c\phi c\psi+\mu\left(\frac{W}{w}-\frac{c\psi}{c\theta}\right)\right]}{L_g^2+\frac{K_\theta}{K_x}-L_g\left[c\theta c\phi s\psi+\mu\left(\frac{W}{w}-\frac{c\psi}{c\theta}\right)\right]} \quad (45)$$

$$\theta_w = \cos^{1}\left(\frac{-B+\sqrt{B^2-4AC}}{2A}\right) \quad (46)$$

with

$$A = W^2 + 2w^2c\phi s\psi\mu$$

$$B = 2w^2c\phi^2c\psi\mu + 2Wwc\phi(1-\mu^2)$$

$$C = w^2c\phi^2(2-\mu^2)$$

Eqs. (45) and (46) describe an approximate linear model of wedging which determines the values of θ_w and s. This linear model is valid only if all three angles (θ, ϕ, ψ) are small (< 5°). In this case, nonlinear terms are infinitesimal when compared with linear terms. We still need to know the admissible range of lateral error, ε_0, on the axis of interest so that we can construct a wedging diagram. In addition, the ratio of K_θ/K_x in eq. (45) appears as a value in the reference frame of the hole and will require a transformation from the frame of the peg.

To find ε_0, let $\tilde{a}$ be the chamfer width. Using the homogeneous transformation matrix, D, in eq. (22) and the geometry of Fig. 4, the admissible range of lateral error for avoiding wedging is:

$$\varepsilon_0 = \tilde{a} + W/2 - (w/2)(c\psi c\phi + s\psi c\theta - s\theta c\psi s\phi) \quad (47)$$

Similarly, the compliance supporting the peg in Fig. 7 is transformed to the frame of the hole.

$$K_x = K_x\, cyc\phi + K_X\,(s\theta c\psi s\phi - s\psi c\theta)$$
$$K_\theta = K_\theta\, c\psi c\phi + K_\phi\,(s\theta c\psi s\phi - s\psi c\theta) + K_\psi\,(s\theta s\psi - c\psi c\theta s\phi) \quad (48)$$

Compliances of the support are denoted by *italic terms*. An approximate wedging diagram shown in Fig. 8 is obtained by making small angle approximations and substituting the following parameters into eq. (45) through eq. (48): ϕ=0°; μ = 1.5, L_g = 1 cm; all linear compliances (K_x and K_y) are 1 N/m; all angular compliances (K_θ, K_ϕ and K_ψ) are 50 N-m/rad.; w = 9 cm, W=10 cm and $\tilde{a}$ = .5 cm.

The solid lines and dashed lines represent the wedging diagram in two dimensions and the approximate three-dimensional wedging diagram, respectively. The diagram considers the effects of three-point contacts. It can be seen that the confined area in the latter case is smaller due to smaller values of θ_w and s. In addition, when the azimuth rotation of the peg, ψ, increases, the admissible range of the lateral error decreases. This means that the wedging space is larger. Therefore, when ψ is small, but non-zero, insertion of square pegs into square holes which leads to the ortho configuration is shown quantitatively to wedge more readily than that of cylindrical pegs and holes of similar support and dimensions.

CONCLUSION

Studies of the peg insertion problem have been carried out for over a decade. The Remote Center of Compliance (RCC), which evolved from the early work, is successful in facilitating peg insertions with tight tolerance. However, its capability is limited to round pegs and holes with chamfers. It fails to insert polygonal, nonsymmetrically-shaped pegs into mating holes. In addition, techniques for using active force control for such mating processes rely on an assumption of predictable initial error due to mating tolerance.

To obtain a better understanding of this problem, we have extended the study of the wedging diagram into three dimensions. Possibilities of wedges for fully-started contacts, e.g., the ortho configuration between a square peg and hole, reveal virtual wedging among three contracts. The wedging space is now described by the parameters of contact configurations: positions and orientations of the peg relative to the hole. Strategies for initially orienting the peg must avoid this wedging space. It remains to determine wedging conditions for other contact configurations and the constraints between them.

REFERENCES

Caine, M. E., 1985, "Chamferless Assembly of Rectangular Parts in Two and Three Dimensions," Master Thesis, Department of Mechanical Engineering, Massachusetts Institute of Technology, Cambridge, MA.

Eppinger, S. and Seering, W., 1987, "Introduction to Dynamic Models for Robot Force Control" *IEEE Control Magazine*, Vol., No. 2.

Faverjon B., and Ponce J., 1991, "On Computing Two-Finger Force-Closure Grasps of Curved 2D Objects," *Proceeding of the 1991 IEEE International Conference on Robotics and Automation*, Sacramento, CA, pp 424-429.

Hunt, K.H., 1978, *Kinematic Geometry of Mechanisms*, Oxford University Press, Oxford, England.

Strip, D. R., 1988, "Insertion Using Geometric Analysis and Hybrid Force-Position Control: Method and Analysis," *Proceedings of the IEEE International Conference on Robotics and Automation*, Philadelphia, PA.

Strip, D. R., 1988, "A Passive Mechanism for Insertion of Convex Pegs," Sandia National Laboratories, Sandia, CA.

Sturges, R. H., 1988, "A Three Dimension Assembly Task Quantification with Application to Machine Dexterity," *The International Journal of Robotics Research*, Vol. 7, pp. 34-78.

Whitney, D. E., 1982, "Quasi-Static Assembly of Compliantly Supported Rigid Parts," *Journal of Dynamic Systems, Measurement, and Control*, Vol. 104, pp. 65-77.

APPENDIX I

Geometric relations involving fixed parameters in Figure 2.

Points 4 and 4' have coordinate (I_x,I_y) and(I'_x,I'_y), respectively:

$$I_x = \frac{d_3 - d_3'}{\left[\tan\left(\alpha - \frac{\pi}{2}\right) - \tan(\alpha + \theta_1)\right]}$$

$$I_y = \frac{d_3 - d_3'}{\left[1 - \frac{\tan(\alpha + \theta_1)}{\tan(\alpha - \frac{\pi}{2})}\right]}$$

$$I_x' = \frac{d_3 - d_3'}{\left[\tan\left(\frac{\pi}{2} - \alpha\right) - \tan(\alpha + \theta_1)\right]}$$

$$I_y' = \frac{d_3 - d_3'}{\left[1 - \frac{\tan(\alpha + \theta_1)}{\tan(\frac{\pi}{2} - \alpha)}\right]}$$

where

$$d_3' = d_2 \tan(\alpha + \theta_1)$$

After knowing these coordinates, θ_{2w} can be determined by using the condition of the normal at the contact point 2:

$$\beta = \theta_{2w} + \tan^{-1}\left(\frac{d_3 - d_4}{d_1 + d_2}\right) - \alpha$$

$$\gamma = \theta_{2w} + \alpha - \tan^{-1}\left(\frac{d_4 - I_y'}{d_1 + I_x'}\right)$$

which leads to eq. (6)

Similarly, we can also obtain the values of β and γ as following.

$$\beta = \theta_{2w} + \tan^{-1}\left(\frac{d_3 - d_4}{d_1 + d_2}\right) - \alpha$$

$$\gamma = \theta_{2w} + \alpha - \tan^{-1}\left(\frac{d_4 - I_y'}{d_1 + I_x'}\right)$$

Note that $(\theta_{2w} - \gamma)$ is the lower bound condition of virtual wedging for the three contact forces along the boundary of friction cones (also see Fig. 2).

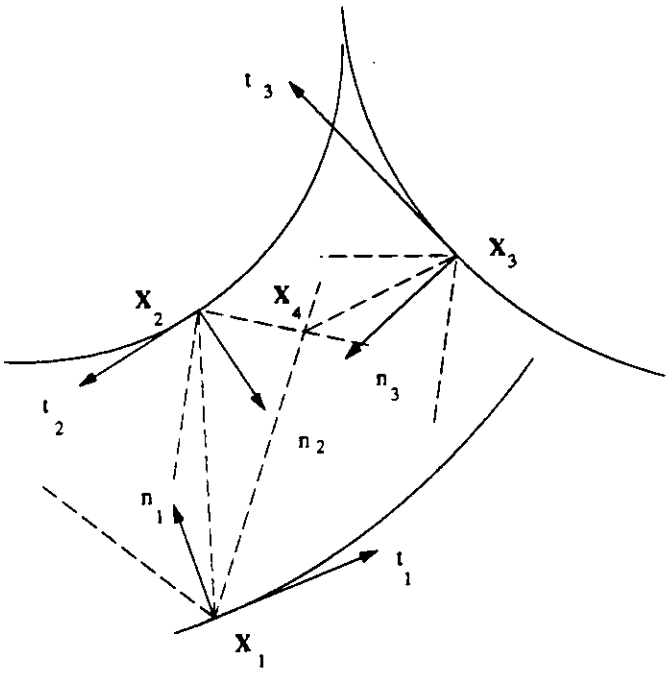

Fig. 1: Generalized three contact configuration with virtual wedging

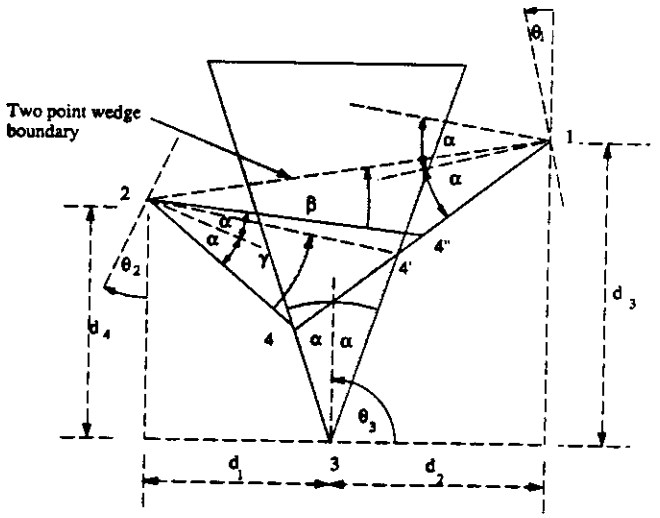

Fig. 2: Virtual wedging in a polygonal geometry

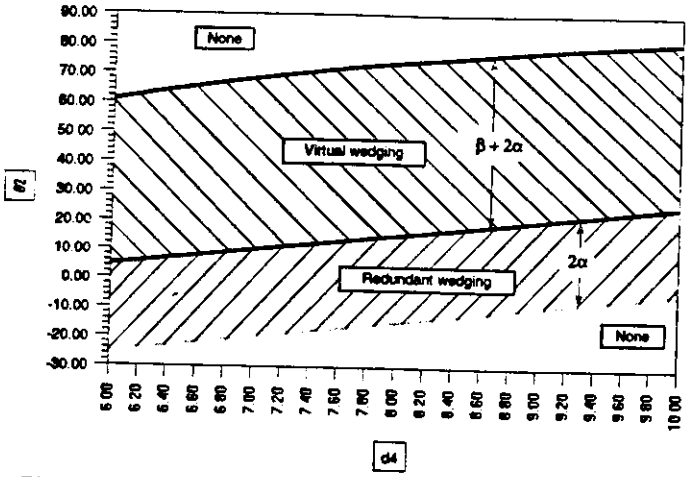

Fig. 3: θ_{2w} of virtual and redundant wedging for the contacts in Fig. 2: $\theta_1 = 20°$, $\theta_3 = 90°$, $\alpha = 15°$ and $d_1 = 4.0$ cm, $d_2 = 7.0$ cm, $d_2 = 8.0$ cm

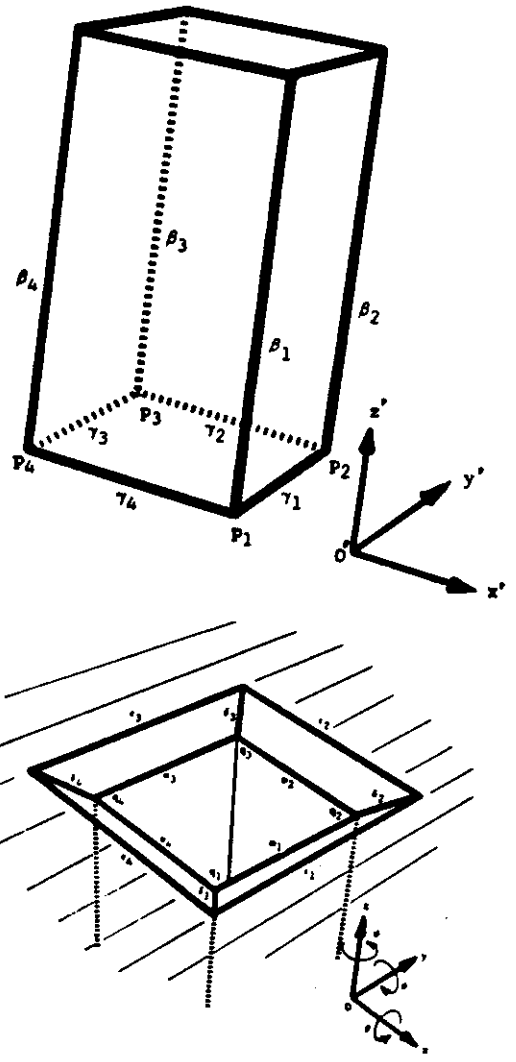

Fig. 4: Feature definitions of a square peg and hole

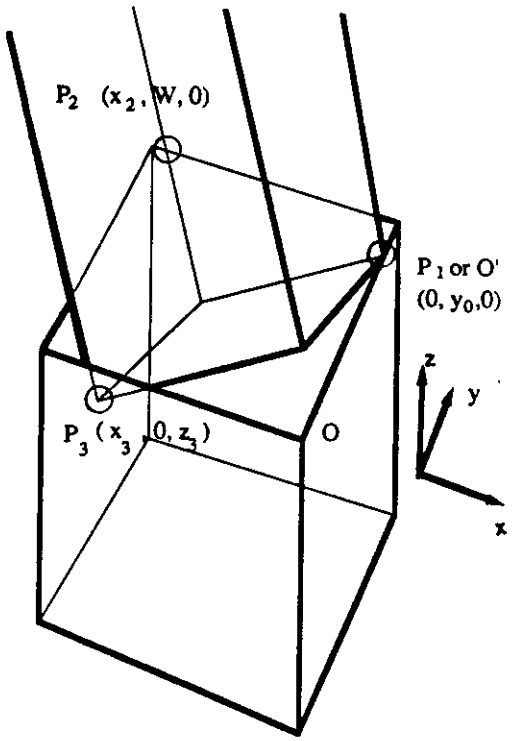

Fig. 5: Ortho configuration at onset of wedging

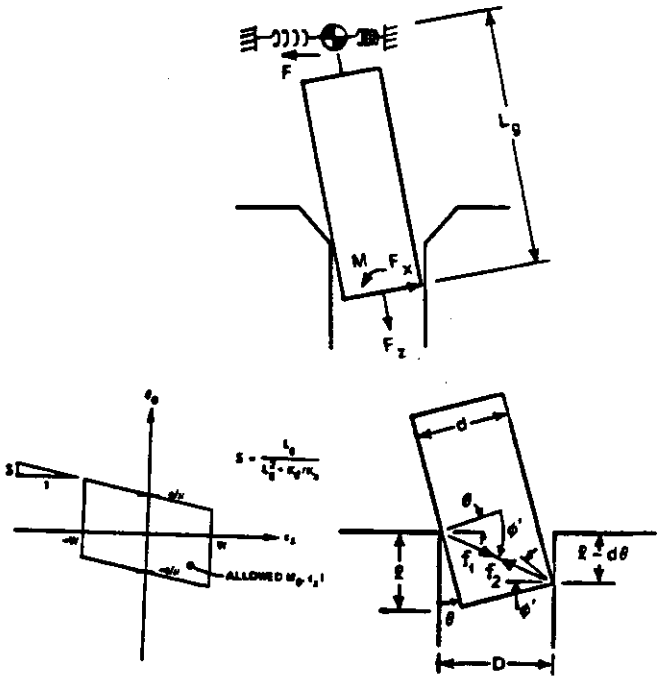

Fig. 6: Wedging diagram for two-dimensional peg insertion tasks

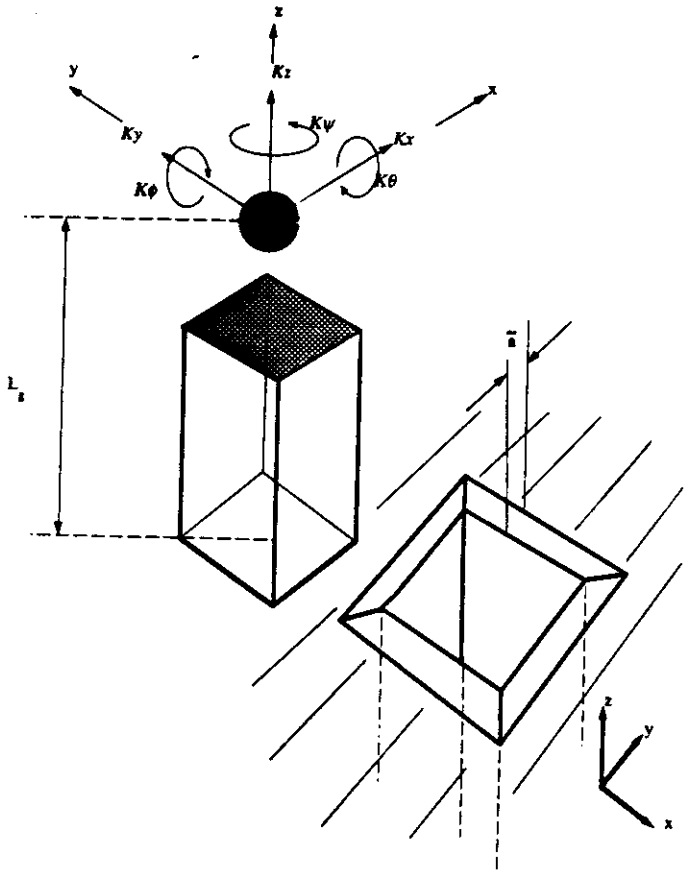

Fig. 7: Generalization of linear and angular compliance of the support

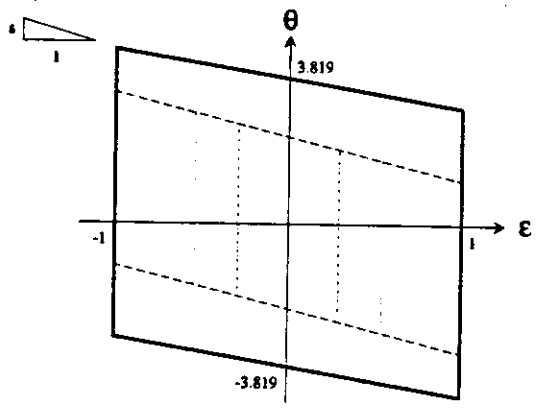

Wedging Diag.	Line symbol	Azimuth angle (ψ) degree	slope	Y- intercept degree	X- intercept cm
Whitney (2D)	———	0	- 0.019	3.819	1
Ortho-Configuration	- - - - -	0	- 0.023	2.457	1
	.....	6			0.55
	- . - . -	10			0.28

Fig. 8: Wedging diagram for the ortho configuration compared with the 2-D case